energies

MDPI

Article

Simulation Study of Single-Adsorber Heat Pump Cycle with Heat Recovery Through Stratified Storage in Both Adsorber and Evaporator/Condenser Loops

Alireza Sadeghlu and Ferdinand P. Schmidt *

Energy and Building Technology Group, Institute of Applied Thermofluidics, Karlsruhe Institute of Technology (KIT), Kaiserstr. 12, 76131 Karlsruhe, Germany; alireza.sadeghlu@kit.edu
* Correspondence: ferdinand.schmidt@kit.edu; Tel.: +49-721-6084-3026

Abstract: A modified single-adsorber cycle for a gas-fired adsorption heat pump (GAHP) is described and analyzed through dynamic simulation with Modelica. The adsorption modules are based on the SAPO-34 / water working pair with parameters taken from a recent R&D project. A stratified storage integrated into the primary heat pump loop is employed for heat recovery of the adsorber as well as the EC heat exchanger (functioning both as an evaporator and condenser). A heating system of a stock multifamily residential building in Germany is assumed as the load to be covered by the heat pump. Representative load points according to VDI 4650-2 and DIN EN 12309-6 rules are considered. The hydraulic system design and implications of the storage integration on degrees of freedom during operation are discussed. The results show that, for a well-stratified storage, similar COP values to a dual-adsorber heat pump cycle based on the same adsorption module type are achievable. Possible additional benefits of the storage are discussed.

Keywords: single-adsorber cycle; dual-adsorber cycle; sensible heat recovery; gas adsorption heat pump; seasonal gas utilization efficiency

Citation: Sadeghlu, A.; Schmidt, F.P. Simulation Study of Single-Adsorber Heat Pump Cycle with Heat Recovery Through Stratified Storage in Both Adsorber and Evaporator/Condenser Loops. *Energies* **2024**, *17*, 5472. https://doi.org/10.3390/en17215472

Academic Editors: Matteo Dongellini and Claudia Naldi

Received: 25 September 2024
Revised: 22 October 2024
Accepted: 25 October 2024
Published: 1 November 2024

1. Introduction

1.1. Research Context

Thermally driven heat pumps are being researched and developed as a means to reduce fossil energy consumption and to cut CO_2 emissions, mostly in the building sector. While absorption heat pumps of the ammonia/water type are market available for larger buildings since several decades, with typical heating powers upwards of 30 kW (see, e.g., [1,2]), adsorption heat pumps have actively been developed over the past 20 years, especially for smaller buildings [3]. Absorption heat pumps mostly rely on the ammonia/water working pair [1], enabling ambient air as the low-temperature heat source even at temperatures below 0 °C. In contrast, there is a broader range of working pairs available for adsorption heat pumps (see, e.g., [4–6]). A key challenge in the development of adsorption heat pumps is to achieve low heat and mass transfer resistances in the adsorber heat exchanger to enable high-volume specific heating powers [3,7]. One particularly promising development route for adsorbers enabling excellent thermal contact between adsorbent and heat exchanger material is the consumptive in situ crystallization of certain alumino-silicates and alumino-phosphates on aluminum substrates [7–9]. Especially the silico-aluminophosphate SAPO-34 can be synthesized via this route [7] and has favorable adsorption properties for chillers and heat pumps with water as the working fluid, namely a high water adsorption capacity [6] and an S-shaped adsorption isotherm with a steep loading increase in the low-relative-pressure range [10,11].

1.2. Project Background

Based on the progress in adsorber development along this route (for the SAPO-34/water working pair) at the company Fahrenheit and its research partners [9,12], it seemed feasible to develop a compact gas-fired adsorption heat pump for multifamily stock buildings, using either a borehole heat exchanger or ventilation exhaust air from the building as the low-temperature heat source.

A key challenge on the system level was to achieve heating supply temperatures of up to 55 °C (at full load), since, for this design temperature, a large fraction of existing radiators in the German multifamily building stock could still be used with the heat pump, thus reducing the renovation costs [13,14]. The temperature lift (between low-temperature source and medium-temperature sink) achievable with the SAPO-34/water working pair is limited to about 30 K, meaning that, with the available low-temperature sources, the adsorption process would not be able to generate the 55 °C supply temperature required at full heating load. It would also not be able to completely supply the domestic hot water (DHW) loads in centralized systems requiring a hot water circulation of, at minimum, 55 °C for hygienic reasons (legionella prevention). Therefore, the system-level design of the adsorption heat pump would require a "direct burner mode" for supplying the peak loads with the highest supply temperature demands. Achievable gas savings on an annual basis would therefore strongly depend on the part-load performance of the adsorption heat pump. This development endeavor was undertaken within the collaborative R&D project "AdoSan" funded by the German federal ministry of economics and climate protection [15].

1.3. Project Results

The main results of that project, including the experimental results on the gas adsorption heat pump (GAHP) demonstrator unit tested at Fraunhofer ISE, have already been reported by our colleagues [16]: the GAHP demonstrator was run under four different cycle conditions, and these experimental results were used to calibrate and validate a numerical GAHP system model in Modelica. Using this validated model, annual simulations of a reference multifamily building were performed and yielded a seasonal gas utilization efficiency (SGUE) of 1.21. When representative load points according to VDI-4650-2 [17] were simulated, the obtained SGUE was 1.26 for a heating system with 55 °C/45 °C design supply and return temperatures [15,16]. Those results provide the reference case for our analysis reported here. Note that the SGUE, as defined in [17], represents the annual ratio of output heat to the input gas heat. In contrast, the seasonal coefficient of performance (SCOP) for electrically driven heat pumps, as detailed in [18], is defined as the ratio of output heat to input electrical energy. Thus, both SGUE and SCOP serve the same function, but they differ in the energy source.

1.4. Cycle Concept Dependency on Adsorption Module Type

There are two distinct adsorption module types, depicted in Figure 1. Within the AdoSan project, the module manufacturer Fahrenheit had a preference for the valveless module type (left in Figure 1) that features a single combined evaporator/condenser (EC) HX and no vapor valve within the vacuum chamber encompassing the adsorber and evaporator/condenser. The other (right) module type has separate evaporator and condenser units, which are each separated from the adsorber chamber through a vapor valve that is designed to open (without external actuation, aided by gravity) upon a positive pressure difference between the bottom and top side.

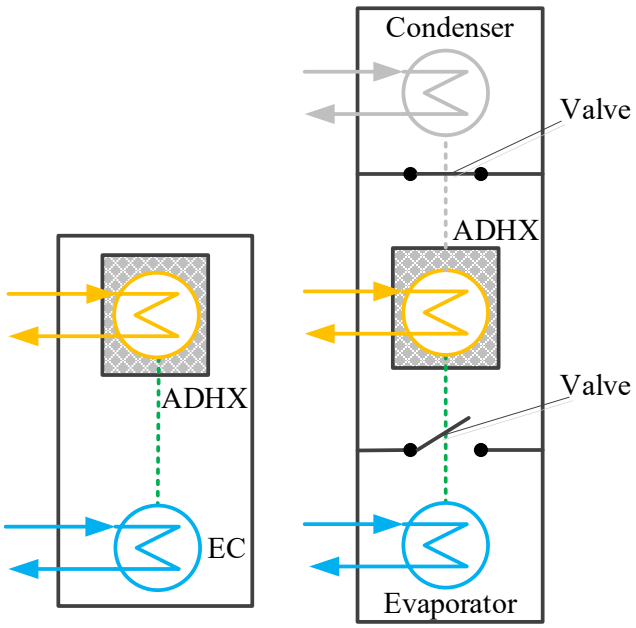

Figure 1. Schematic comparison of two adsorption modules types (depicted during adsorption process): the adsorber/desorber (ADHX) in the right module is connected to separate evaporator and condenser units, with valves positioned between them. In contrast, in the left module, the adsorber/desorber and the combined evaporator/condenser (EC) are placed within the vacuum chamber with no valves between them. (Blue lines indicate the low-temperature source loop; orange lines represent the medium-temperature sink loop; green dash lines show water vapor; and grey lines denote inactive components).

Regarding achievable GAHP performance (assuming perfect operation of the vapor valves), the valveless module type (left) is at a disadvantage since it requires the external switching of the EC HX between the low-temperature source loop (when functioning as an evaporator) and the medium-temperature sink loop (when functioning as a condenser), involving a sensible heat required to heat the EC HX from the evaporator to condenser temperature after each adsorption half cycle.

The AdoSan GAHP demonstrator unit was based on a dual-adsorber cycle, in which two identical valveless adsorption modules were operated alternatively [16]. The hydraulic scheme is shown in Figure 2. For dual-adsorber cycles, there are efficient ways for a (partial) recovery of the abovementioned sensible heat between the two EC heat exchangers of the two adsorption modules [19]. For the AdoSan unit, a delayed return flow switching of both the adsorbers and the EC heat exchangers is employed for heat recovery [20–22]. In contrast, in single-adsorber cycles (as reported here), heat recovery is possible only through integrated storage, since there is no second module available operating with a phase shift to the first module. A single-adsorber cycle concept dubbed "Stratisorp" was previously developed in our group [23–26], which relies on the coupling of the adsorber to a stratified storage equipped with inlet stratifiers and multi-way valves for extracting fluid from different heights in the storage. Note that, in this Stratisorp cycle, only the adsorber is connected to a stratified storage. During the adsorption process, both sensible and sorptive heat from the adsorber are stored in the storage to reuse during the desorption process. In this concept, the lowest temperature within the stratified storage (at its bottom layer) is the return flow temperature of the heat sink loop. Under favorable conditions, including very good stratification in the storage, this approach can lead to a heat recovery higher than that achievable with the two-adsorber cycle described above, enabling high COP values [25]. However, this only works well for the module type with separate evaporator and condenser heat exchangers (right in Figure 1). When the other (left) module type is

used in a Stratisorp cycle, the sensible heat of the EC HX (at temperatures below that of the heating return flow) cannot be recovered for the lack of a storage option.

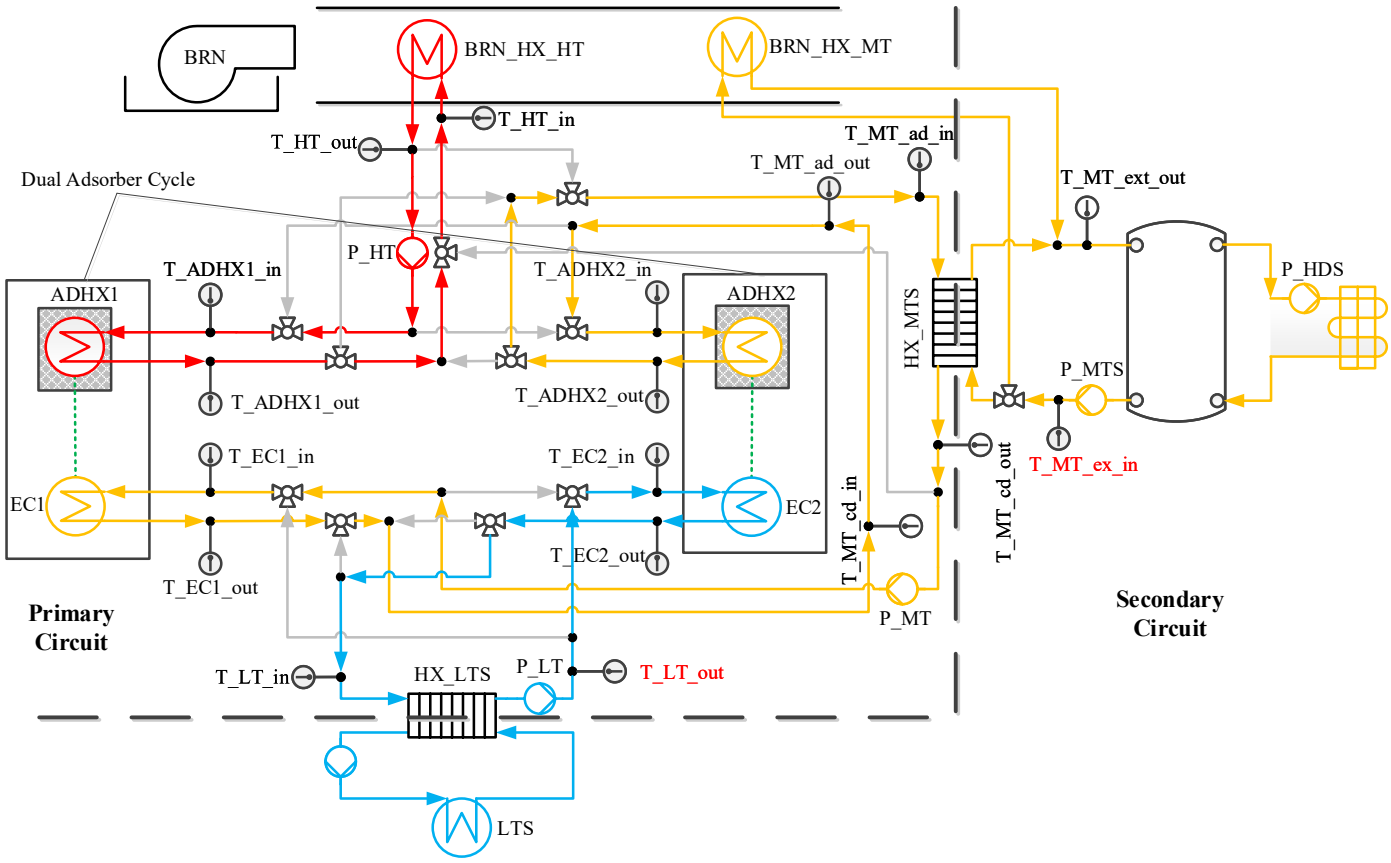

Figure 2. Hydraulic scheme of heating system with dual-adsorber cycle (reference) GAHP, shown during desorption of left and adsorption of right module; red lines represent the high-temperature source loop; blue lines show the low-temperature source loop; orange lines present the medium-temperature sink loop; green dash lines show water vapor; and grey dash lines show currently inactive connections.

In the single-adsorber cycle presented in this study, both the ADHX and EC HX are connected to the stratified storage, as shown in Figure 3. The innovation lies in utilizing the lowest part of the stratified storage to store heat at temperatures below the heating return flow. This configuration enables heat recovery in both adsorber and EC loops. The rationale for this research lies, on the one hand, in potential cost savings of a single-adsorber heat pump, and, on the other hand, in the flexibility and adaptability of a single-adsorber cycle coupled to a stratified storage. Our main objective here is to find a single-adsorber configuration (with a hydraulic scheme and control scheme) that achieves an SGUE as high as possible with the same adsorber configuration (and same adsorbent mass per kW of nominal power of the heat pump) as in the reference system. Our simulation results should serve as a proof of concept for the hydraulic scheme and as a starting point for further control optimizations.

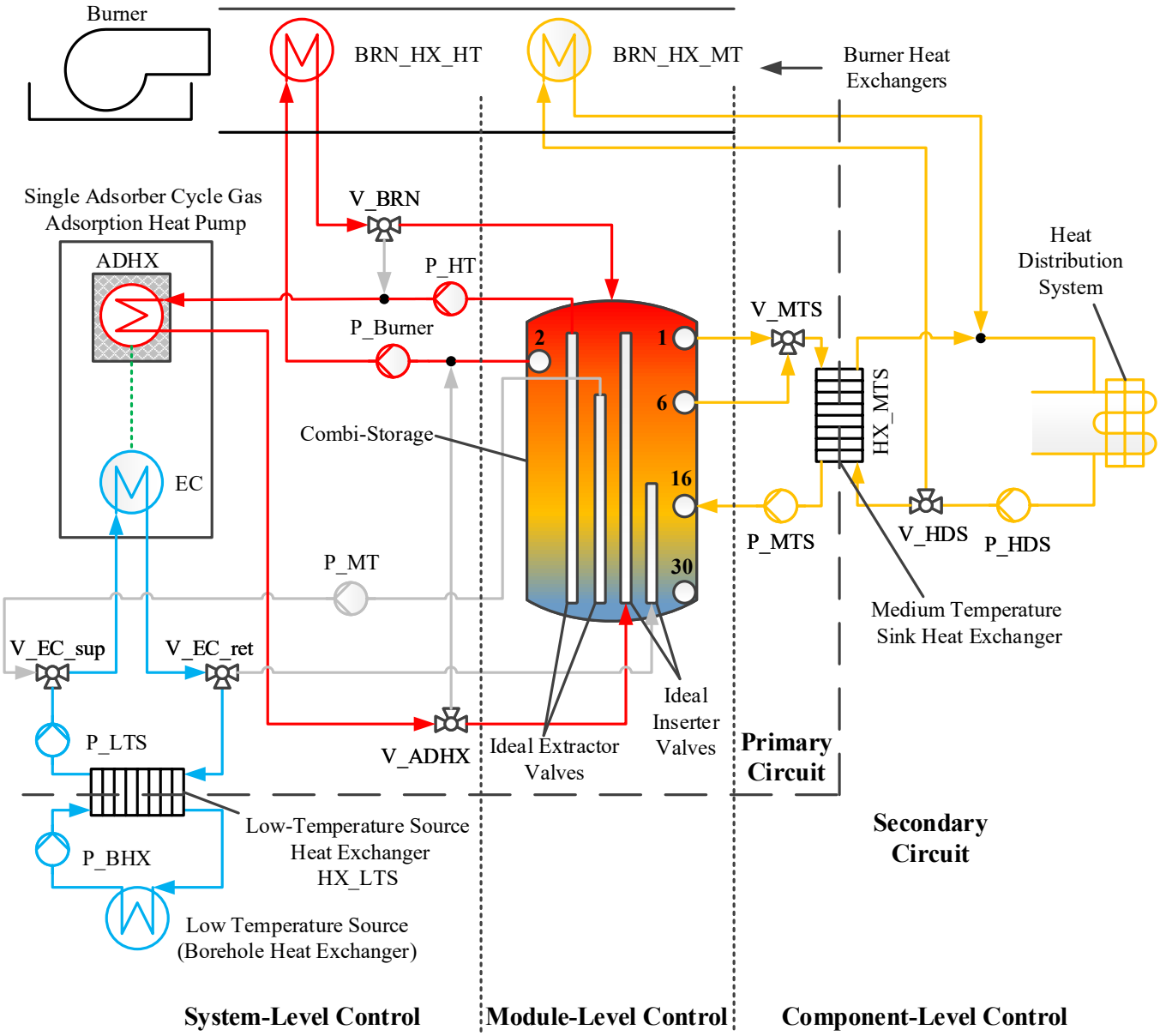

Figure 3. Hydraulic scheme of heating system with single-adsorber cycle GAHP (shown during desorption phase); red lines represent the high-temperature source loop; blue lines show the low-temperature source loop; orange lines depict the medium-temperature sink loop; green dash line shows water vapor; and grey lines show currently inactive connections.

2. Method

2.1. System Sizing with Respect to Reference System

In the AdoSan GAHP demonstrator and its validated model [16], the design power of the GAHP was 40 kW, i.e., 20 kW per adsorption module. Since we are using that same pre-validated component model of the adsorption module in our analysis of a single-adsorber cycle, we set the GAHP design power to 20 kW, i.e., both our nominal heating load and nominal burner power are set to 20 kW. However, in this research, the mass flow rates of the adsorber and condenser have additional degrees of freedom due to the decoupling from the sink mass flow enabled by the integration of the stratified storage tank.

2.2. System Description

Both in our single-adsorber system as seen in Figure 3 and the reference GAHP (Figure 2), the primary circuit is distinctly isolated from the secondary circuit by the

medium-temperature sink HX and the low-temperature source HX. Also, both systems feature a burner with two heat exchangers (BRN_HX_HT and BRN_HX_MT), of which the latter one is, in both systems, directly integrated into the medium-temperature sink (MTS) loop. Its function is to cool the flue gas below its dew point (achieving condensation) and to transfer the extracted heat directly to the secondary circuit (heat sink).

The integration of the first heat exchanger BRN_HX_HT) differs between the two systems. While, in the dual-adsorber GAHP, it is symmetrically connected to both adsorption modules to be able to heat either of them during desorption, in the single-adsorber GAHP, it can be linked either to the upper part of the storage or to the adsorber, acting as a high-temperature source.

Note that the storage in Figure 3 is an integral part of the heat pump system, which is integrated into its primary fluid loop. In contrast, in the dual-adsorber cycle [15,16,27], the storage is typically positioned on the other side of the medium-temperature sink heat exchanger, as depicted in Figure 2. Therefore, in our single-adsorber system, the storage serves a dual role: internal heat recovery within the cycle and buffering for loads. The role as a buffer storage is however not analyzed further within this contribution, since only stationary load points are considered here. Beyond the scope of this work, it is envisioned that the storage could at the same time serve as a storage for DHW preparation, i.e., act as a combi-storage.

The stratified storage is connected to the single-adsorber cycle GAHP through four multi-way valves, which are modeled here as ideal extraction and insertion from/into specific layers of the storage. The adsorber and the EC HX are each connected to a pair of these valves. Additionally, for switching the connection of the EC HX between stratified storage and borehole heat exchanger as a low-temperature heat source, two three-way valves (V_EC_sup and V_EC_ret in Figure 3) are located in the supply and return lines and operate in the following modes: during the desorption process, both valves are connected to the stratified storage. In this mode, supply water is extracted from the stratified storage via an ideal extractor and directed to the condenser. Then, the heated water is inserted into the storage through an ideal inserter. At the end of the desorption process, a transition mode to adsorption occurs. During this transition, both three-way valves remain connected to the stratified storage to transfer sensible heat from the condenser to the stratified storage. This is achieved by changing the EC HX set point temperature from space heating supply temperature to the storage bottom-layer temperature in 180 s intervals, as described in Table 1.

Table 1. Transition modes between desorption and adsorption processes.

Sequence	Time [s]	Set Point (Desorption to Adsorption)	Set Point (Adsorption to Desorption)
1	60	Space Heating Return Temperature	Bottom-Layer Temperature
2	60	Bottom-Layer Temperature Plus 2 °C	Bottom-Layer Temperature Plus 2 °C
3	60	Bottom-Layer Temperature	Space Heating Return Temperature

Subsequently, during the adsorption process, the two three-way valves (V_EC_sup and V_EC_ret in Figure 3) connect the EC HX (now functioning as an evaporator) to the low-temperature source (LTS-HX) to take up energy from the borehole HX, within a temperature range of 6 °C to 9 °C [17]. Finally, at the end of the adsorption process, a transition mode from adsorption to desorption occurs to heat the EC HX, as described in Table 1. During this mode, the two three-way valves (V_EC_sup and V_EC_ret in Figure 3) reconnect to the stratified storage in order to raise the EC HX temperature to the space heating return temperature and recover the stored sensible heat.

2.3. System Modeling

The Modelica system model employed in this study is a dynamic model that attempts to capture multiple physical aspects of the real system: adsorption equilibria of the working

pair, heat and mass transfer resistances within the adsorption module, thermal masses of the components, heat losses to the ambience, and heat flows within components due to thermal bridges. Our model directly builds on that of the dual-adsorber reference system, described in detail in [16]. More details on model assumptions (especially regarding heat and mass transfer) are provided in [27] and in the PhD thesis of A. Velte [21] (in German).

In this research, a single-adsorber cycle, utilizing a borehole heat exchanger as a low-temperature heat source, is integrated with a space heating circuit. The supply and return temperatures for the borehole heat exchanger and space heating circuit are specified in Table 2 to maintain room temperature within comfort range. Heat production and heat consumption are connected through a one-cubic-meter stratified storage tank with default 30 layers to have the same simulation condition as the AdoSan's heating system. Selecting a stratified storage has been carried out based on available water extraction technologies, such as movable extractor [28], thermo-differential [29], multi-way, and integrated valves, which support precise temperature layer management and enhance system efficiency. These components are numerically constructed using sub-models from publicly available libraries for Dymola, which is a commercial modeling and simulation tool for systems modeled in Modelica. These libraries include Buildings-Library [30], AixLib [31], IBPSA [32], and SorpLib [33], which are employed to analyze the simulation model for this research. For each boundary condition described in Table 2, the model was simulated over three days until the results stabilized and exhibited periodicity. Periodicity is achieved when the system state at the end of cycle n is equivalent to the state at the end of cycle $n + 1$. A three-day simulation is generally sufficient for equilibration. Within the last ten cycles, the fluctuation in GUE is always less than 0.3%. Then, the last cycle was extracted for the evaluation.

Table 2. The part-load ratios and temperature boundary conditions for the secondary hydraulic circuit in Figure 3 include supply and return temperatures for the heating system. These temperatures are specified for heating circuit design temperatures of 45/55 °C (according to VDI 4650-2 [17]) and 41/55 °C (according to DIN EN 12309-6 [34]).

Number	Part-Load Ratio DIN EN 12309-6 (%)	Return in °C DIN EN 12309-6	Supply in °C DIN EN 12309-6	Part-Load Ratio VDI 4650-2 (%)	Return in °C VDI 4650-2	Supply in °C VDI 4650-2	Borehole Heat Exchanger Inlet in °C
6	**100**	41	55	**100**	45	55	5
5	**73**	37.1	47.6	**63**	37.2	43.4	5
4	**58**	34.7	43.1	**48**	33.8	38.5	6
3	**46**	31.9	38.2	**39**	31.7	35.6	7
2	**31**	29	33.2	**30**	29.6	32.6	8
1	**15**	25.4	27.4	**13**	24.8	26	9

2.4. Control Strategy

There are three layered control strategies for the heating system with a single-adsorber cycle GAHP, as shown in Figure 3. The first layer operates at the component level, controlling certain components, such as the mass flow rate of the pumps (P_HDS and P_MTS), the mixing valve V_MTS with a PI controller, and splitting valve V_HDS. The second layer operates at the module level, switching the extraction and insertion valves (from/to the stratified storage) according to temperature criteria. In this way, the adsorption, desorption, and transition processes are being controlled. The third layer operates at the system level, supervising the mass flow rate of pumps based on module-level conditions. It also controls the burner's operation mode, either heating the upper part of the storage to supply space heating demand when the heat pump cannot or disconnecting from the storage and

connecting to the desorber to sustain the desorption process. Each level is discussed in detail below.

2.4.1. Component-Level Control

The nominal mass flow rate of different components for the reference system and single-adsorber cycle system are provided in Table 3. The three-way valve V_MTS (cf. Figure 3) fulfills the function to maintain the required supply temperature to the heat distribution system. It is connected to layers 1 and 6 of the stratified storage and mixes the two flows by means of a PI controller, in this case, using the supply temperatures specified in VDI 4650-2 [17] or DIN EN 12309-6 [34] for renovated buildings as set points.

The three-way splitting valve V_HDS is controlled to maintain a mass flow rate of 0.1 kg/s through BRN_HX_MT when the burner is active. This is carried out to achieve the condensing boiler effect despite the high fluid temperatures in the first heat exchanger. A sensitivity analysis conducted during the AdsoSan project for the reference system had shown that this low mass flow was sufficient to extract the heat of condensation and that system efficiency was not very sensitive to the exact mass flow value [15].

Table 3. Nominal mass flow rate of different components in reference system [16] and single-adsorber cycle system.

Nominal Mass Flow Rate [kg/s]	Reference GAHP	Single-Adsorber Cycle GAHP
Burner	0.67	0.35
Adsorber/Desorber	0.67	0.35
Condenser	0.67	0.5
Evaporator	0.94	0.5
BRN_HX_MT	0.1	0.1

2.4.2. Module-Level Control

On the module level, there are separate temperature-based controls for the extractor valves of the condenser and adsorber using different set-point temperatures depending on the cycle phase. During the desorption phase, the water extracted in the supply line to the condenser is set to match at least the return temperature of the space heating circuit (based on VDI 4650-2 [17] or DIN EN 12309-6 [34] standards and the specific representative operating points in Table 2). A bit later in the cycle, when the desorber is heated directly from the burner, the condenser extraction temperature set point is set to the supply temperature of the space heating circuit. This is mainly because the condenser temperature has a degree of freedom in a single-adsorber cycle GAHP as opposed to a dual-adsorber cycle GAHP. Therefore, a temperature difference (T_des − T_cond) of approximately 40 K, which is defined as temperature thrust, is sufficient for the desorption process. This indicates potential for enhancing efficiency by increasing the condenser temperature during the final desorption step, as shown in the time series of the average temperatures of the adsorber/desorber and evaporator/condenser for a cycle in Section 3.

In the single-adsorber cycle with a valveless module (left in Figure 1), the working fluid always flows between the adsorber/desorber and EC, even during the supposedly isosteric phases of the cycle. This fluid flow is especially pronounced when the temperatures of the two components do not align precisely with the isosteric temperature profile. Therefore, it is important to avoid the loss of cooling capacity through synchronously cooling both the condenser and the desorber during the transition mode from desorption to adsorption. To achieve this, the temperature set point of the condenser undergoes a series of changes over a 180 s period (Table 1) to push warm water from the condenser into the stratified storage. The length and steps of this transition period have been determined by trial and error and thus could be further optimized.

Conversely, during the transition mode from adsorption to desorption, the temperature levels are adjusted to push the cold water from the evaporator into the stratified storage over 180 s (Table 1).

Before explaining the control logic of the ideal extractor valve for the adsorber/desorber, it is important to note that the bottom part of the stratified storage is designated for heat recovery between the evaporator and condenser, which corresponds to the temperature range between the borehole HX and the space heating circuit return temperature. The middle part of the stratified storage is designated for buffering heat for the sink loop, covering the temperature range between the supply and return temperatures of the space heating circuit. Finally, the top part of the stratified storage is designated for buffering heat above the supply temperature, as shown in the color spectrum of the storage in Figure 3. Thus, the module-level control strategy evaluates two distinct conditions through the ideal extractor valve to regulate the adsorption and desorption processes within the single-adsorber cycle.

In the adsorption process (after the abovementioned transition phase), the adsorber is gradually cooled through the storage. The ideal extractor valve is controlled such that it always extracts the warmest water that is at least 2 K colder than the mean adsorbent temperature. Meanwhile, the evaporator is connected to the borehole HX, taking up ambient heat. This process continues until the set point temperature reaches the space heating return flow temperature. Once this transition condition is met, adsorption continues at the current extraction level until the temperature difference between the adsorber outlet and inlet falls below 1 K. Then, the transition phase into desorption is entered.

During the first part of the desorption phase, heat is supplied to the desorber from the stratified storage, while the condenser transfers heat to the stratified storage. During this phase, the control system selects the coldest layer that is at least 2 K warmer than the mean adsorbent temperature. This process continues until the condition reaches the top storage layer. When there is no hotter storage layer available to satisfy the condition, the desorber is connected to the burner and the desorption process continues until the desorber output temperature exceeds 90 °C. Then, the cycle restarts.

Schwamberger [25] showed for the Stratisorp cycle that higher driving temperature differences lead to higher cycle powers. However, we adopted a simple approach and chose a 2 K temperature difference between the adsorber/desorber and storage selected layer. Thus, improved control could vary this value based on load fraction.

Furthermore, the return water from the condenser and adsorber/desorber is directed to the layer in the stratified storage with the closest temperature through ideal inserters, located in the return line of the adsorber/desorber and condenser heat exchangers.

2.4.3. System-Level Control

The concept of system-level control is based on the fact that the space heating demand may not be satisfied with the heat pump for high load points, since the burner can only heat the single desorber during the cycle fraction corresponding to the last desorption step. When this is the case, the burner operates for an extended period to charge the storage directly. This “direct heating mode” of the storage by the burner is activated in the system-level controls when the topmost storage layer temperature is lower than a specific set point temperature. For this “direct heating”, water is extracted from the second highest level in the storage and reinserted into the top level after passing through the burner HX. When the adsorber extraction index valve reaches the top layer of the storage and the layer temperature matches the set point temperature, the burner is shifted from heating the upper part of the stratified storage to the desorber viaV_BRN and V_ADHX in Figure 3. Furthermore, the system-level control monitors the mass flow rate of the adsorber/desorber pump and reduces it only during each of the two 180 s transition phases.

2.5. Energy and Entropy Balance

Since our Modelica model builds on the GAHP model of the reference system that is described in detail in [16], our readers are kindly referred to that paper for the energy balances of all components except for the stratified storage (which is given below). We here focus on the entropy balance of a single-adsorber cycle and especially the stratified storage. An entropy balance for the "Stratisorp" single-adsorber cycle was previously given by Schwamberger [25,26]. His model was implemented in MATLAB (R2015b), which allowed him to separate the plug flow in the storage from the thermal mixing and to separately calculate the mixing entropy. Since we have found no such way to separate these effects in our Modelica model, the entropy balancing described below differs from Schwamberger's account. A detailed discussion of different sources of irreversibility in a stratified storage can be found in [35].

2.5.1. Stratified Storage

The numerical model of the stratified storage tank, referred to as 'Stratified' from the Buildings Library [30], is based on the ideal plug flow assumption, with no additional mixing model except in cases of temperature inversion, which is addressed by natural mixing due to buoyancy effects. This modeling approach is commonly employed in system simulations with stratified storage tanks, as demonstrated in [36]. For this study, we have chosen to use this model with 30 layers, which is a higher number than that commonly used. The lower the number of layers, the greater the numerical dissipation generated, so a model with fewer layers can roughly mimic the effect of convective mixing in a storage tank. Our intention here is to analyze a very-well-stratified storage in order to determine the potential of this cycle type (independent of effects of poor stratification). Our understanding is that existing stratification devices and extraction valves would need to be adapted and/or improved to achieve the level of stratification exhibited by our model in practical applications.

A schematic of an n-layer stratified storage tank is illustrated in Figure 4. Each layer contains a unique volume and three fluid ports. Port one is used as the water inlet for the layer, port two is used as the outlet, and port three is used for the extraction or insertion of water from a particular layer. Additionally, each layer transfers heat to the environment and adjacent layers through its thermal resistance. The energy balance for the stratified storage tank, assuming that layer 1 is the hottest and layer n the coldest, can be expressed as follows:

$$\begin{cases} \text{Storage:} \\ CV_1 : \sum(\dot{m}_{\text{in}} h_{\text{in}})_1 - \sum(\dot{m}_{\text{out}} h_{\text{out}})_1 - \dot{Q}_{1,2} - \dot{Q}_{1,env} = \dfrac{dE_1}{dt} \\ CV_2 : \sum(\dot{m}_{\text{in}} h_{\text{in}})_2 - \sum(\dot{m}_{\text{out}} h_{\text{out}})_2 + \dot{Q}_{1,2} - \dot{Q}_{2,3} - \dot{Q}_{2,env} = \dfrac{dE_2}{dt} \\ \qquad . \\ \qquad . \\ \qquad . \\ CV_n : \sum(\dot{m}_{\text{in}} h_{\text{in}})_n - \sum(\dot{m}_{\text{out}} h_{\text{out}})_n + \dot{Q}_{n-1,n} - \dot{Q}_{n,env} = \dfrac{dE_n}{dt} \end{cases} \tag{1}$$

The source of irreversibilities in each layer is the finite temperature differences between layers and the mass transfer between them. The entropy balance for a system undergoing any process can be expressed in terms of the rate as follows [37]:

rate of net entropy transfer by mass + rate of net entropy transfer by heat
+ rate of entropy generation = rate of change in the Entropy

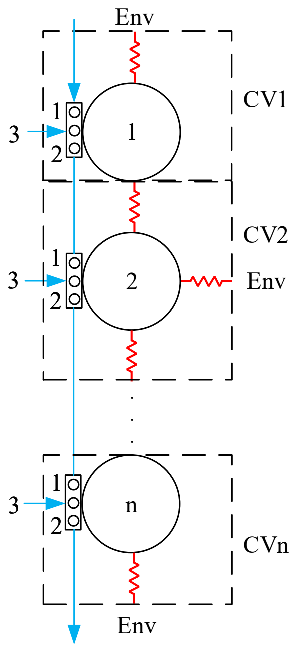

Figure 4. Resistance-capacitance model with control volumes for an n-layer stratified storage. $\dot{m}_{1,1}$: External flow into CV1, $\dot{m}_{1,3}$: external flow into or out of CV1, $\dot{m}_{1,2}$: flow out from CV1, $\dot{m}_{2,1}$: flow into CV2 from CV1, and, etc., $\dot{m}_{n,2}$: flow out of CVn.

$$\begin{cases} \text{Storage:} \\ CV_1 : \sum(\dot{m}_{\text{in}} s_{\text{in}})_1 - \sum(\dot{m}_{\text{out}} s_{\text{out}})_1 - \dfrac{\dot{Q}_{1,2}}{T_1} - \dfrac{\dot{Q}_{1,env}}{T_{env}} + \dot{S}_{1,gen} = \dfrac{dS_1}{dt} \\ CV_2 : \sum(\dot{m}_{\text{in}} s_{\text{in}})_2 - \sum(\dot{m}_{\text{out}} s_{\text{out}})_2 + \dfrac{\dot{Q}_{1,2}}{T_1} - \dfrac{\dot{Q}_{2,3}}{T_3} - \dfrac{\dot{Q}_{2,env}}{T_{env}} + \dot{S}_{2,gen} = \dfrac{dS_2}{dt} \\ \vdots \\ CV_n : \sum(\dot{m}_{\text{in}} s_{\text{in}})_n - \sum(\dot{m}_{\text{out}} s_{\text{out}})_n + \dfrac{\dot{Q}_{n-1,n}}{T_n} - \dfrac{\dot{Q}_{n,env}}{T_{env}} + \dot{S}_{n,gen} = \dfrac{dS_n}{dt} \end{cases} \tag{2}$$

In the Modelica framework, the sign of a flow variable, such as mass flow rate, changes automatically when the flow direction changes. Similarly, the sign of an across variable, such as heat transfer, changes automatically depending on whether heat is entering or leaving the system. This accurately represents dynamic systems where both flow directions and heat transfer may vary over time.

2.5.2. Single-Adsorber Components

The R-C (resistance–capacitance) diagram with control volumes is depicted in Figure 5 and defined in Table 4. Each capacitance represents the thermal mass of the materials and each resistance represents a particular heat transfer mechanism, including a mix of radiation, conduction, and convection. The entropy balances of the respective control volumes are given below.

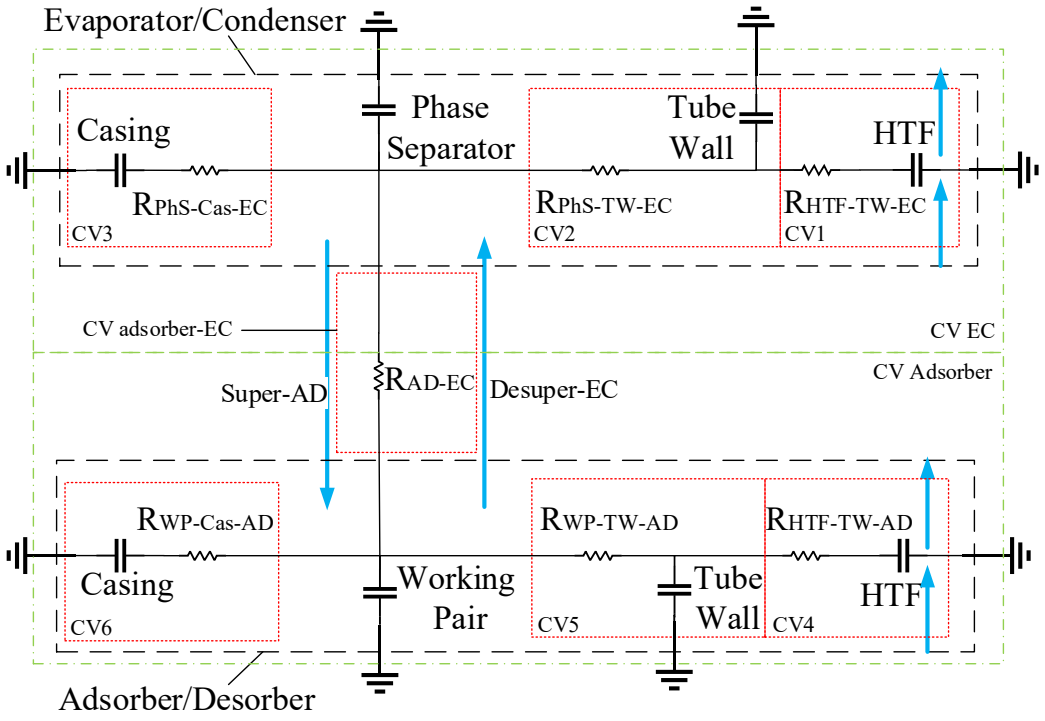

Figure 5. Resistance-capacitance model with control volumes for a single-adsorber cycle. Black rectangles indicate the boundaries of the adsorber/desorber and evaporator/condenser components, while green rectangles represent their control volumes. The red rectangles highlight the irreversibility source in the single-adsorber cycle. Blue arrows on the right-hand side show the heat transfer fluid inside the pipes, with the central section illustrating the superheating and desuperheating states of the working fluid.

Table 4. Different elements of R-C model for a single-adsorber cycle.

Symbol	Definition
HTF-TW-EC	Resistance between Heat Transfer Fluid and Tube Wall in the Evaporator/Condenser
PhS-TW-EC	Resistance between Phase Separator and Tube Wall in the Evaporator/Condenser
PhS-Cas-EC	Resistance between Phase Separator and Casing in the Evaporator/Condenser
AD-EC	Resistance between Adsorber/Desorber and Evaporator/Condenser
Desuper-EC	Desuperheat in the Evaporator/Condenser
Super-AD	Superheat in the Adsorber/Desorber
WP-Cas-AD	Resistance between Working Pair and Casing in the Adsorber/Desorber
WP-TW-AD	Resistance between Working Pair and Tube Wall in the Adsorber/Desorber
HTF-TW-AD	Resistance between Heat Transfer Fluid and Tube Wall in the Adsorber/Desorber

$$\begin{cases} \text{Evaporator/Condenser:} \\ CV_1 : (\dot{m} * s)_{\text{HTF,in}} - (\dot{m} * s)_{\text{HTF,out}} + \dfrac{\dot{Q}_{\text{HTF,Tube Wall}}}{T_{\text{Tube Wall}}} + \dot{S}_{HTF,\text{gen}} = \dfrac{dS_{\text{HTF}}}{dt} \\ CV_2 : + \dfrac{\dot{Q}_{\text{HTF,Tube Wall}}}{T_{\text{Tube Wall}}} + \dfrac{\dot{Q}_{\text{Tube Wall,Phase Separator}}}{T_{\text{Phase Separator}}} + \dot{S}_{\text{Tube Wall,gen}} = \dfrac{dS_{\text{Tube Wall}}}{dt} \\ CV_3 : \dfrac{\dot{Q}_{\text{Casing,Phase Separator}}}{T_{\text{Phase Separator}}} - \dfrac{\dot{Q}_{\text{Casing,environment}}}{T_{\text{Casing}}} + \dot{S}_{\text{Casing,gen}} = \dfrac{dS_{\text{Casing}}}{dt} \end{cases} \quad (3)$$

$$\begin{cases} \text{Between Evaporator/Condenser and Adsorber:} \\ CV_{\text{Desuperheat}} : \dot{m}_{\text{adsorber}} \left(s_{\text{in,adsorber}} - s_{\text{out,EC}} - \left(\frac{h_{\text{in,adsorber}} - h_{\text{out,EC}}}{T_{\text{EC}}} \right) \right) + \dot{S}_{\text{Desuperheat,gen}} = 0 \\ CV_{\text{Superheat}} : \dot{m}_{\text{EC}} \left(s_{\text{in,EC}} - s_{\text{out,adsorber}} - \left(\frac{h_{\text{in,EC}} - h_{\text{out,adsorber}}}{T_{\text{adsorber}}} \right) \right) + \dot{S}_{\text{Superheat,gen}} = 0 \\ CV_{\text{adsorber-EC}} : \frac{\dot{Q}_{\text{adsorber,EC}}}{T_{\text{adsorber}}} - \frac{\dot{Q}_{\text{adsorber,EC}}}{T_{\text{EC}}} + \dot{S}_{\text{adsorber-EC,gen}} = 0 \end{cases} \tag{4}$$

$$\begin{cases} \text{Adsorber:} \\ CV_4 : (\dot{m} * s)_{\text{HTF,in}} - (\dot{m} * s)_{\text{HTF,out}} \overset{+}{-} \frac{\dot{Q}_{\text{HTF,Tube Wall}}}{T_{\text{Tube Wall}}} + \dot{S}_{HTF,\text{gen}} = \frac{dS_{\text{HTF}}}{dt} \\ CV_5 : \overset{-}{+} \frac{\dot{Q}_{\text{HTF,Tube Wall}}}{T_{\text{Tube Wall}}} \overset{+}{-} \frac{\dot{Q}_{\text{Tube Wall,Working Pair}}}{T_{\text{Working Pair}}} + \dot{S}_{\text{Tube Wall,gen}} = \frac{dS_{\text{Tube Wall}}}{dt} \\ CV_6 : \frac{\dot{Q}_{\text{Casing,Working Pair}}}{T_{\text{Working Pair}}} - \frac{\dot{Q}_{\text{Casing,environment}}}{T_{\text{Casing}}} + \dot{S}_{\text{Casing,gen}} = \frac{dS_{\text{Casing}}}{dt} \end{cases} \tag{5}$$

$$RI_{\text{i}} = \frac{\dot{S}_{i,gen}}{\dot{S}_{tot,gen}} = \frac{\dot{S}_{i,gen}}{\dot{S}_{Adsorber,gen} + \dot{S}_{EC,gen}} \tag{6}$$

3. Results

The idealized standard cycle of an adsorption heat pump consists of two isosteres and two isobars [38]. However, in any real system, isosteric phases do not occur due to the heat capacity of the metal and the water inside of the evaporator and condenser [38]. In real systems using the module type with a separate evaporator and condenser (right in Figure 1), the switching phases between adsorption and desorption approximate isosteric behavior. Conversely, in systems with a single EC and no internal vapor valves, mass transfer within the module continuously occurs during the switching phases, leading to a larger deviation from isosteric behavior [38].

In the following, we will discuss the simulation results of the single-adsorber cycle for the 30% load point according to VDI 4650-2 in some detail. The Clausius–Clapeyron diagram of that whole cycle is shown in Figure 6, which shows the pre-cooling affected by the transition of the EC HX described above and the simultaneous cooling of the adsorber. Note that this pre-cooling is facilitated by the flexibility of connecting the single-adsorber cycle GAHP to the stratified storage, allowing the condenser temperature to drop from the heating supply temperature to the temperature of the storage bottom layer over a 180 s interval, as shown in the second plot of Figure 7.

The pre-cooling process stores the available heat from the condenser in the storage. If this heat is not stored, some of the condensation heat during the next desorption process will be used to achieve the necessary sensible heating of the condenser to reach the space heating return temperature. However, by storing and using this heat, a greater amount of condensation heat remains within the useful temperature range, thereby improving the performance. During the pre-cooling, a 180 s transition phase occurs by extracting water from storage at a low mass flow rate to cool down the desorber, while the mass flow rate of the condenser remains unchanged. However, the condenser temperature levels changes, as shown in Table 1. The results of the 180 s transition phase, as presented in Table 5 and Figure 6, show that the pre-cooling does not conclude at the end of this period. Then, the condenser connects to the borehole HX and cools down to the evaporator temperature by the end of the pre-cooling process. Furthermore, the pre-cooling process causes a portion of the previously condensed working fluid to evaporate and be adsorbed by the adsorbents, which reduces the condenser temperature.

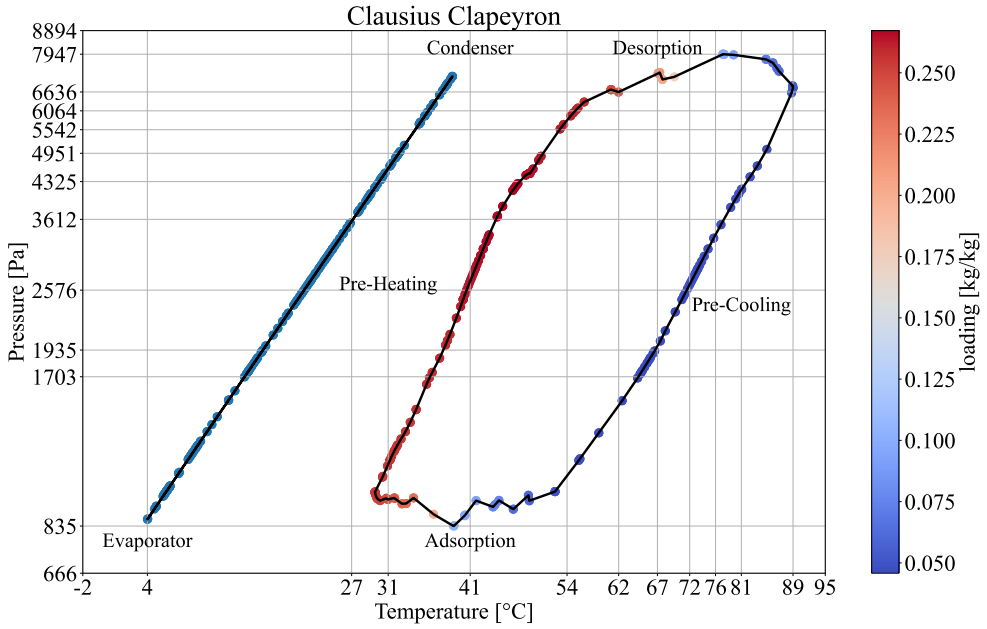

Figure 6. Variation in pressure, temperature, and loading for a working pair. These data correspond to a heating system integrating with a single-adsorber cycle GAHP operating at a 30% part-load ratio (refer to Table 2) for a single cycle, with the maximum high-temperature source set at 90 °C.

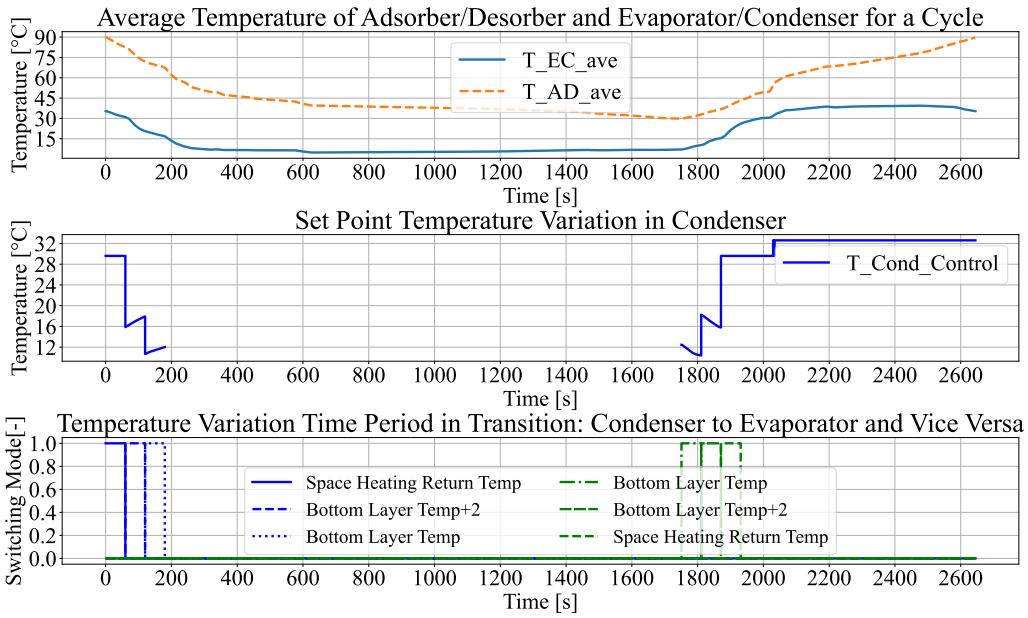

Figure 7. Time series of the average temperatures of the adsorber/desorber and evaporator/condenser, as well as the condenser set point temperatures for the ideal extractor valve in the supply line of the evaporator/condenser, and the activation time period of the valve during transition mode. These data correspond to a heating system integrating with a single-adsorber cycle GAHP operating at a 30% part-load ratio (refer to Table 2) for a cycle, with the maximum high-temperature source set at 90 °C.

Table 5. Desorber and condenser conditions during 180 s transition for the 30% load point according to VDI 4650-2.

Time Point	Desorber		Condenser	
	Temperature (°C)	Pressure (Pa)	Temperature (°C)	Pressure (Pa)
Start	89.7	6834	35.4	5750
End	67.3	1913	16.9	1920

The coefficient of performance and power density of GAHPs must be balanced as a trade-off [15,21,25]. As a result, the adsorption process starts with a low adsorption rate, as indicated by the loading plot in Figure 8. This low rate is due to the extraction water from a high-temperature layer (T1 in Figure 8), which is a compromise for effective heat recovery. Then, inserting water from the lower-temperature layer of storage into the adsorber increases the driving temperature between the adsorber and stratified storage, subsequently enhancing the rate of adsorption. One observation from Figure 6 is that there is a notable pressure drop during adsorption close to an adsorber temperature of 40 °C. This is related to the S-shaped water adsorption isotherm of SAPO-34 and occurs at the final adsorption step, when the drop in temperature of the fluid extracted from the storage strongly shifts the adsorption equilibria, leading to an increase in adsorption rate (at 600 s in Figure 8). The pronounced variation in pressure during the ideally isobaric adsorption and desorption phases also indicates that the EC HX is undersized relative to the adsorber. However, this is not necessarily a design flaw, since, for the single-EC module type, there is always a trade-off between the total heat transfer and thermal mass of the EC HX [39], making a relatively small evaporator HX a rational choice in some cases.

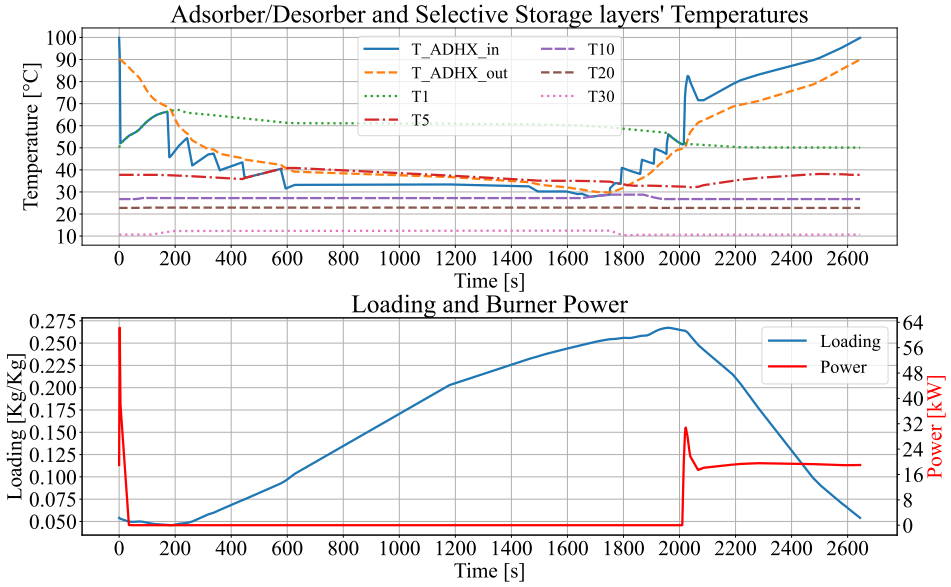

Figure 8. Time series of heat transfer fluid supply and return temperatures for the adsorber, stratified storage representative layers' temperatures, loading, and burner power. These data correspond to a heating system integrating with a single-adsorber cycle GAHP operating at a 30% part-load ratio (refer to Table 2) for a cycle, with the maximum high-temperature source set at 90 °C.

During the pre-heating phase, the evaporator temperature must reach the condenser temperature. Thus, the evaporator connects to the storage. A 180 s transition phase occurs by extracting water from storage at a low mass flow rate to heat up the adsorber, while the mass flow rate of the evaporator remains unchanged. However, the evaporator temperature level changes, as shown in Table 1. The results of the 180 s transition phase, as presented in Table 6 and Figure 6, show that pre-heating does not conclude at the end of this period.

The pre-heating process causes some of the working fluid within the adsorbents to desorb and flow to the evaporator, which increases the evaporator temperature to reach the space heating return temperature, explaining why the pre-heating process is not an isosteric process.

Table 6. Adsorber and evaporator conditions during 180 s transition for the 30% load point according to VDI 4650-2.

Time Point	Adsorber		Evaporator	
	Temperature (°C)	Pressure (Pa)	Temperature (°C)	Pressure (Pa)
Start	29.8	982	7.1	1010
End	43.4	3135	26.1	3377

Figure 9 clearly shows that the heat recovery occurs during transition modes between the evaporator and condenser in a single-adsorber cycle, which is connected to the stratified storage tank. In the first transition mode, the condenser heat is delivered to the storage, resulting in the bottom-layer temperatures increasing. In contrast, during the second transition mode, cold water is delivered to the storage, resulting in a decrease in the bottom-layer temperatures.

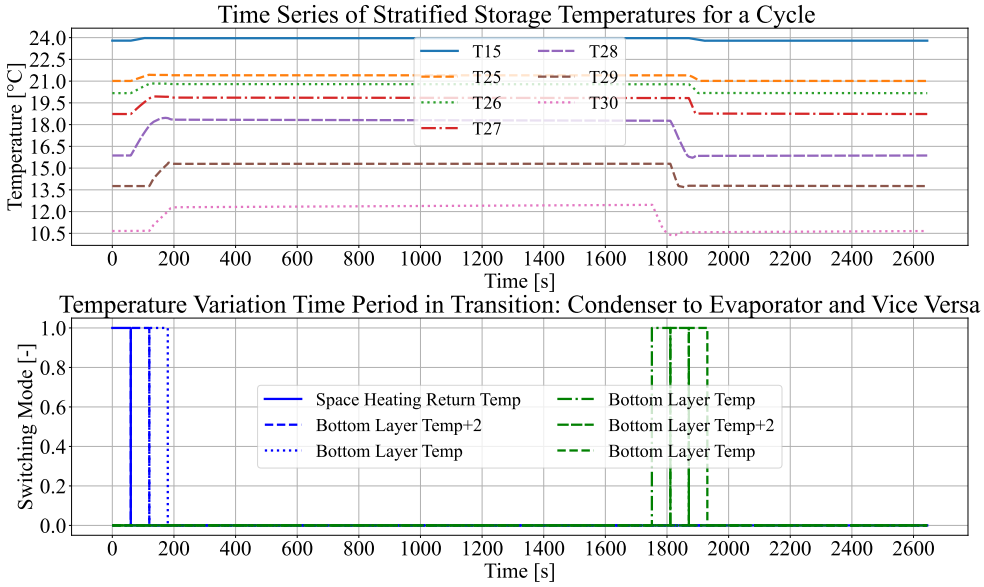

Figure 9. Time series of stratified storage layers' temperatures for layer 15 and six bottom layers and the activation time period of the condenser set point temperatures for the ideal extractor valve in the supply line of the EC during transition mode. These data correspond to a heating system integrating with a single-adsorber cycle GAHP operating at a 30% part-load ratio (refer to Table 2) for a cycle, with the maximum high-temperature source set at 90 °C.

Similar to the beginning of the adsorption process, during the desorption process, Figure 6 shows that the desorber pressure is above the condenser's saturation pressure, which continues until sufficient condensation occurs to reduce the pressure in the desorber. As the extraction index approaches the first layer with the highest temperature, the desorption process requires a higher water temperature to proceed effectively. Consequently, the burner is activated and connected to the desorber, as represented by the red plot in Figure 8. This activation results in a noticeable increase in pressure, as demonstrated in Figure 6. The connection between the desorber and the burner remains until the desorber outlet temperature reaches 90 °C. At this point, one cycle completes.

When the desorber outlet temperature reaches 90 °C, the burner turns off and connects to the stratified storage. As the burner's metal is still hot, the temperature difference between the burner and the storage causes a spike in power due to high conduction heat transfer at the beginning of a cycle, as shown in the time series of the burner power in Figure 8.

Following the module-level control strategy, if the temperature difference between the mean adsorbent temperature and the inlet water temperature is less than 2 °C, the extraction layer is altered. Consequently, the inlet temperature to the adsorber/desorber changes during an adsorber cycle as shown in Figure 8. Moreover, the plot shows that the stratified storage layer temperatures increase during adsorption, while they decrease during desorption. It is also evident from Figure 8 that the desorption phase is significantly shorter than the adsorption phase, which not only serves as an efficient parameter to maximize COP and power density [40] but is also contrary to the behavior observed in the reference GAHP [16].

The adsorber power time series within a cycle is depicted in Figure 10. It shows that the first 180 s are associated with the transition mode from the desorption to adsorption process. Subsequently, the adsorption process takes place. After another 180 s, a transition mode from adsorption to the desorption process occurs, followed by the desorption process to complete a cycle of processes. In the second plot, the extraction and insertion of water from stratified storage into the adsorber/desorber are presented. Finally, the last plot illustrates the inlet and outlet heat transfer fluid temperature within the EC. The closely matched inlet and outlet water temperature at the end of each 180 s transition mode justifies the selection of a 180 s duration for transition phases.

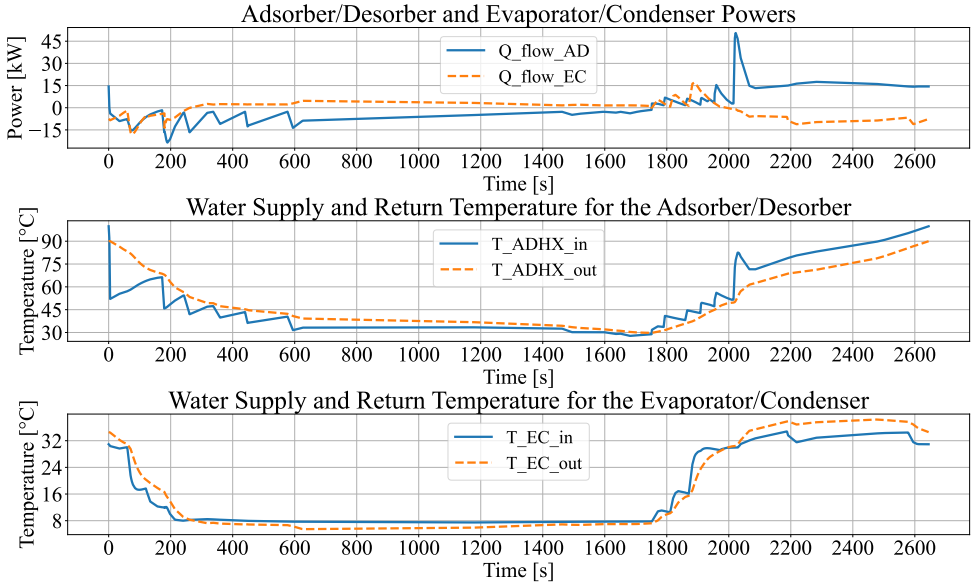

Figure 10. Time series of power, supply, and return temperatures of heat transfer fluid for a module. These data correspond to a heating system integrating with a single-adsorber cycle GAHP operating at a 30% part-load ratio (refer to Table 2) for a single cycle, with the maximum high-temperature source set at 90 °C.

Comparing the loading and power for representative operating points with a partial load of 30% in Figure 8 and a partial load of 48% in Figure 11 reveals two primary outcomes.

First, the maximum loading of the adsorption process reduces, which prevents the layers from attaining sufficient heating through the adsorption process to use in the desorption process.

Second, the burner activation period extends for high partial loads to heat the upper section of the storage and fulfill the heating demand in the consumption section. Therefore,

at the partial load of 48%, the storage layer 1 temperature is set to the space heating supply temperature plus 8 to ensure that the space heating demands are met under this condition.

Since the stratified storage tank is designed to maintain conditions similar to the reference system [15] for comparison with the single-adsorber cycle GAHP and is not sized for hot water preparation and heating buffer functions, these outcomes lead to suboptimal thermal stratification, with certain layers exhibiting negligible temperature variations, as shown in Figure 12.

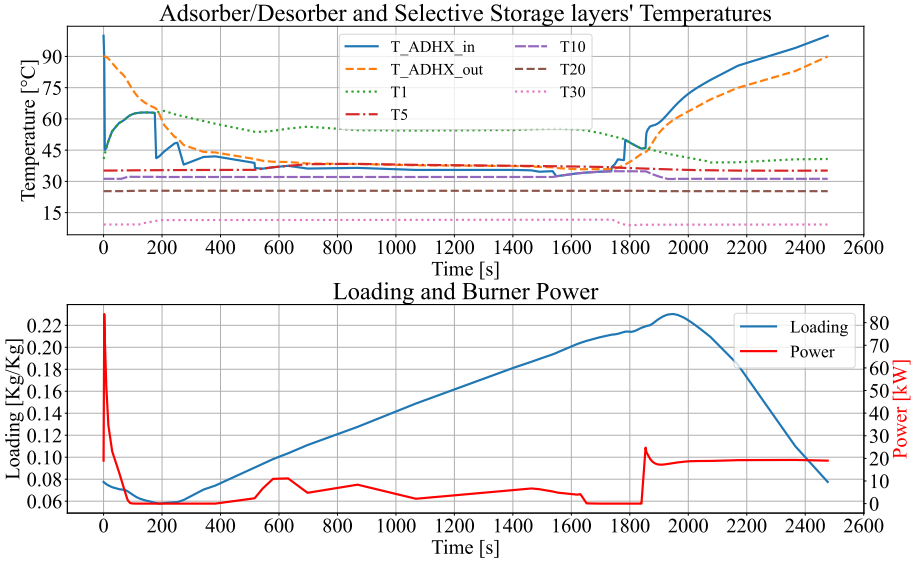

Figure 11. Time series of heat transfer fluid supply and return temperatures for the adsorber, stratified storage representative layers' temperatures, loading, and burner power. These data correspond to a heating system integrating with a single-adsorber cycle GAHP operating at a 48% part-load ratio (refer to Table 2) for a cycle, with the maximum high-temperature source set at 90 °C.

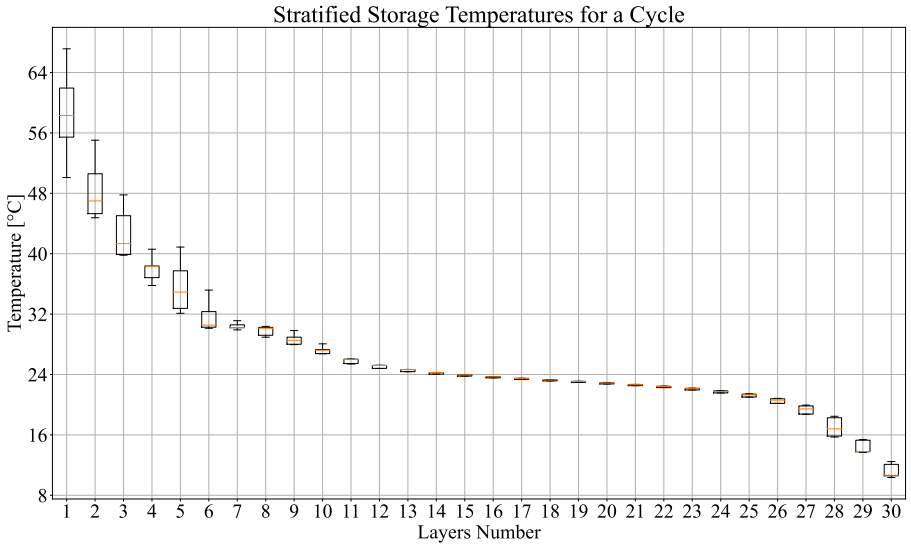

Figure 12. Stratified storage layers' temperatures for a heating system integrating with a single-adsorber cycle GAHP operating at a 30% part-load ratio (refer to Table 2) for a single cycle, with the maximum high-temperature source set at 90 °C.

The entropy balance for main components of the single-adsorber cycle system is shown in Figure 13. The highest spike in the adsorber/desorber is related to the direct burner mode. When the desorption process finishes, the burner turns off and connects to the storage. Therefore, the high temperature difference between the burner and storage leads

to the high entropy generation at the beginning of the cycle, as shown in the second plot of Figure 13. Additionally, the sources of relative irreversibility within the adsorber/desorber are detailed in Figure 14. It reveals that the largest portion is related to "HTF-TW-AD", which represents heat and mass transfer inside the pipe between the heat transfer fluid and tube wall in the adsorber/desorber. This finding aligns with Meunier's results, which defined this phenomenon as external thermal coupling between isothermal heat reservoirs and temperature varying within the adsorber/desorber [41]. The second-largest portion is "AD-EC", denoting heat transfer between the adsorber/desorber and EC. The third-largest portion is "HTF-TW-EC", representing heat and mass transfer inside the pipe between the heat transfer fluid and tube wall in the EC. Finally, the fourth-largest portion is "WP-TW-AD", indicating heat transfer between the working pair and tube wall in the adsorber/desorber.

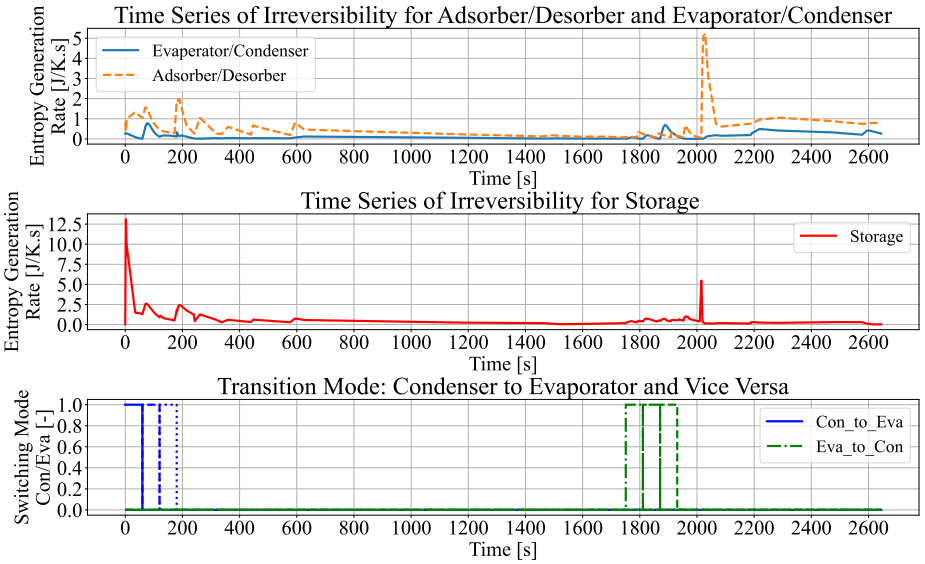

Figure 13. Time series of entropy generation rate within module and storage, as well as transition mode from condenser to the evaporator and vise versa. These data correspond to a heating system integrating with a single-adsorber cycle GAHP operating at a 30% part-load ratio (refer to Table 2) for a single cycle, with the maximum high-temperature source set at 90 °C.

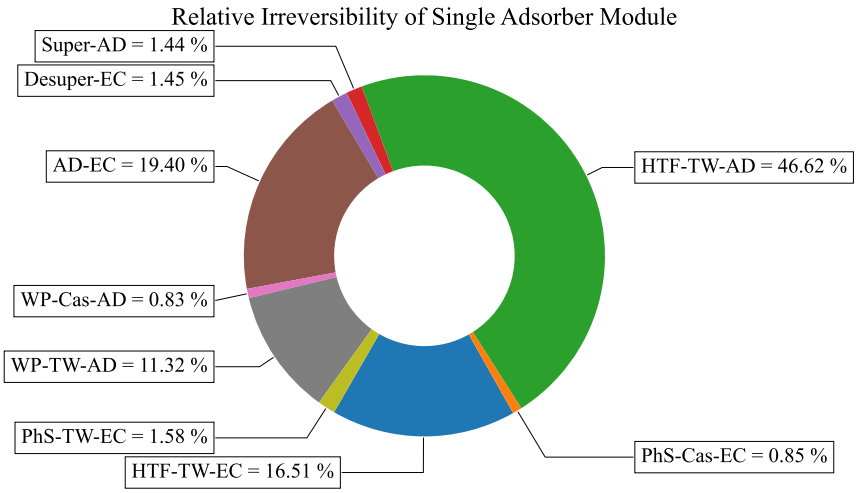

Figure 14. Relative irreversibility for distinct elements within a module. These data correspond to a heating system integrating with a single-adsorber cycle GAHP operating at a 30% part-load ratio (refer to Table 2) for a single cycle, with the maximum high-temperature source set at 90 °C. The abbreviations of the entropy contributions are found in Table 4.

3.1. Gas Utilization Efficiency Compared to Reference System

The seasonal gas utilization efficiency (SGUE) of a heating system integrated with a single-adsorber cycle GAHP and stratified storage has been computed according to two distinct standards, DIN EN 12309-6 [34] and VDI 4650-2 [17], based on the net calorific value (NCV). The results are then compared with the SGUE of a heating system integrated with the dual-adsorber cycle GAHP and hydraulic separator (reference system) in Figure 15. The variation in SGUE values for the same heating system, assessed under VDI 4650 2 [17] and DIN EN 12309-6 [34], can be attributed to the distinctive calculation methodologies employed in these two standards. VDI 4650 2 [17] considers five points, excluding 100% from Table 2, and computes the harmonic mean value based on these five points. Conversely, DIN EN 12309-6 incorporates six points and determines efficiency through a weighted average, including 100%. Consequently, VDI 4650 2 [17] tends to predict SGUE optimistically, while DIN EN 12309-6 [34] tends to predict it pessimistically. This divergence in prediction methods between the two standards is also documented in the reference system assessment for the dual-adsorber cycle GAHP [16]. The observed differences arise from variations in the weighting or selection of different partial load points. Specifically, the weather data utilized for the Potsdam site result in a greater number of operating hours at lower part-load points in VDI 4650 2 [17] compared to what is assumed in DIN EN 12309-6 [34].

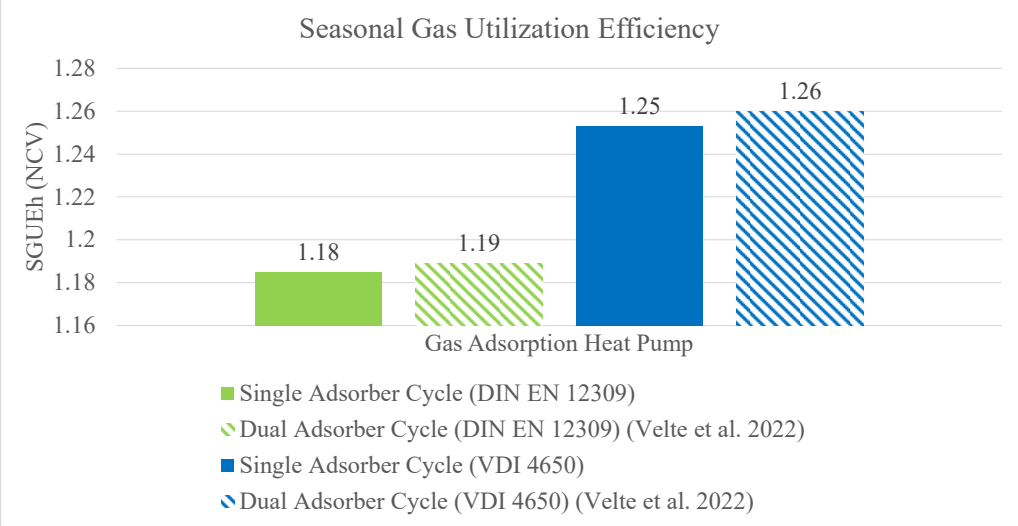

Figure 15. Comparison of the seasonal gas utilization efficiency of a heating system with a single- and dual-adsorber cycle GAHP, assessed by two standards: VDI 4650-2 [17] and DIN EN 12309-6 [34].

Sensitivity Analysis: Desorption Temperature and Flow Rate

The sensitivity analysis of the single-adsorber cycle GAHP consists of two parts. Firstly, the alteration of the high-temperature source from 90 °C to 110 °C, and secondly, doubling the mass flow rate of the burner and adsorber while keeping the high-temperature source at 90 °C. Figure 16 provides the results of the gas utilization efficiency for each part-load ratio mentioned in Table 2 for VDI 4650-2 [17].

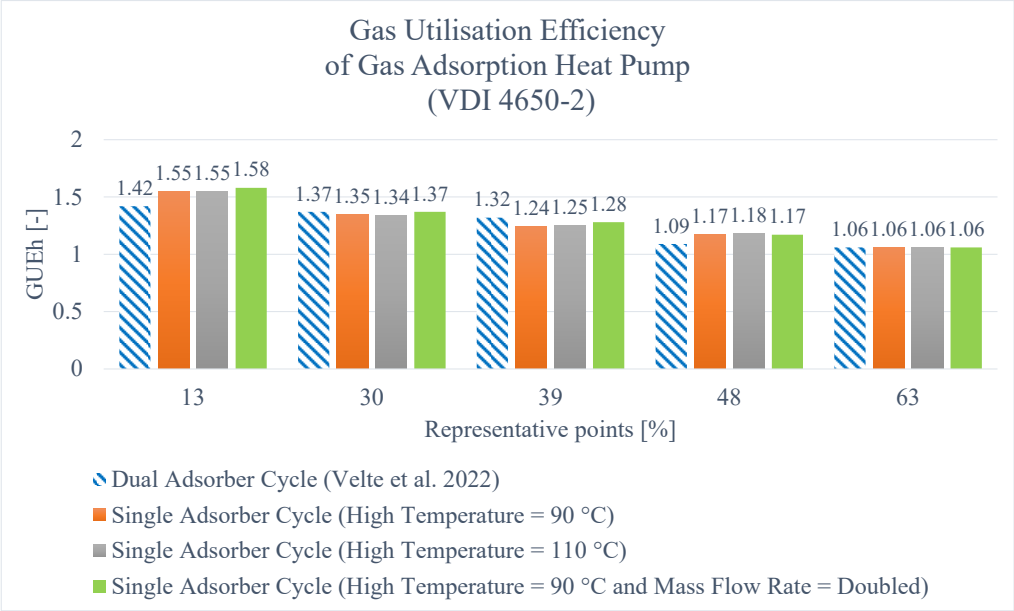

Figure 16. Gas utilization efficiency of a heating system: sensitivity analysis with heat production involving a single- and dual-adsorber cycle GAHP, and heat consumption is based on representative operating points specified in the VDI 4650-2 standard [17]. The reference system high temperature is 90 °C.

3.2. Seasonal Gas Utilization Efficiency

Figure 17 illustrates the SGUE in a heating system integrated with a single-adsorber cycle GAHP and stratified storage under three different sensitivity analyses, comparing it with the reference system including a dual-adsorber cycle [16]. The results indicate that doubling the mass flow rate in the burner and adsorber leads to a higher SGUE than the validated model. This improvement is primarily attributed to the increase in gas utilization efficiency by 11.3% for the 13% part-load ratio and 7.3% for the 48% part-load ratio, while decreasing by 3% for the 39% part-load ratio in Figure 16. This shows that there is still room for optimizing mass flow controls and fully utilizing this degree of freedom in storage-integrated single-adsorber cycles.

3.3. Remarks on Scalability and Adaptability of System

The degrees of freedom of the storage-coupled single-adsorber cycle with regard to adsorber and EC mass flows as well as storage layer switching rules should make it highly adaptable to different operating conditions and/or adsorber properties or even working pairs. However, there is not yet a systematic understanding of how to design the system controls to make the best use of these degrees of freedom. Tuning the controls for this system involved some trial and error, and we would very much welcome further work of control experts on this system. Regarding the chosen heating supply design temperature of 55 °C, it should be relevant to a significant fraction of buildings in many countries where similar types of radiators are employed and similar building insulation standards are applied as in Germany. The VDI 4650-2 and DIN EN 12309-6 rules provide a suitable framework for a relatively simple prediction of seasonal gas utilization efficiencies, although deviations from the results of full annual simulations can be significant [16].

Scaling to different powers for larger or smaller buildings should be relatively straightforward. When the storage size is scaled with the nominal heating power, storage size might become the limiting factor for finding installation space at higher heating powers.

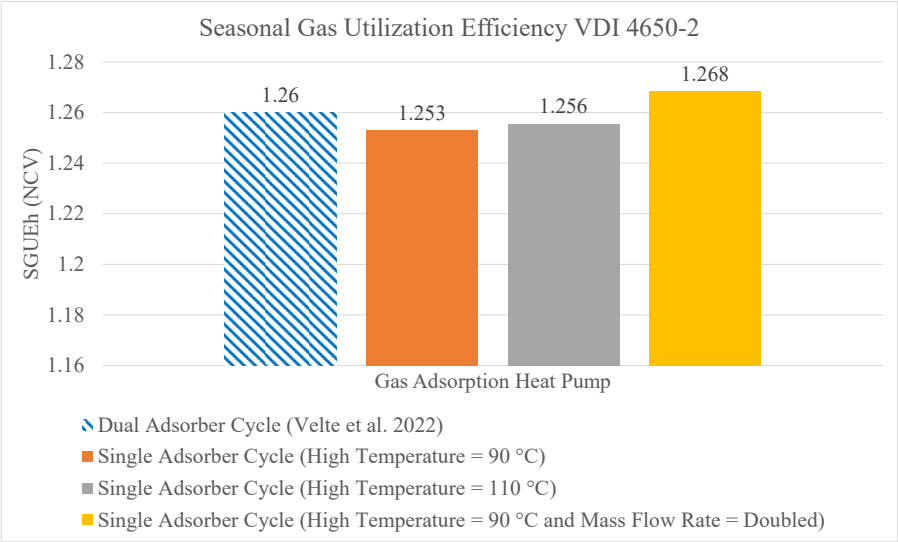

Figure 17. Seasonal gas utilization efficiency of a heating system: sensitivity analysis with heat production involving a single-adsorber cycle GAHP and heat consumption based on representative operating points specified in the VDI 4650-2 standard [17].

4. Summary and Conclusions

A simulation study was conducted in this research. The simulated heating system includes a single-adsorber cycle GAHP with a borehole HX as a low-temperature heat source and a burner as a high-temperature heat source, with space heating in a stock multifamily residential building as the only heat sink. A stratified storage tank is tightly integrated into the adsorption cycle, and an innovative coupling of both the adsorber and the evaporator/condenser HX to the stratified storage enables heat recovery from both heat exchangers within the cycle. The storage is modeled here by a simplified plug-flow model without a specific mixing model, and this model is parameterized with 30 layers in order to obtain a well-stratified storage for a study of the technical potential of the system (without effects from poor stratification). Accordingly, the fluid extraction valves and stratification devices for fluid reinsertion into the storage are assumed as ideal. A layered control strategy is presented and shown to achieve the desired sensible heat recovery between the evaporation and condensation phases A comparison with a reference system with a dual-adsorber cycle GAHP [16] reveals the flexibility of the single-adsorber cycle: the adsorber mass flow rate has a degree of freedom in this system (due to the decoupling from the sink mass flow enabled by the storage). Increasing the mass flow has been shown to increase system performance under some load conditions. The overall performance of the system (in terms of the SGUE) is very similar to the dual-adsorber reference system.

Future work should focus on further improving the control strategy, making good use of the flexibility enabled by the storage integration, e.g., through intra-cycle mass flow variation. Both experimental and simulation work on stratification and mixing in the storage under more realistic conditions are still needed. The system's flexibility could be utilized to an even higher degree if the adsorber and/or evaporator/condenser cycle were adapted to the operating conditions: the hardware required for this system would also allow for running modified cycles like a "double lift" or "enhanced efficiency" cycle [42]. These are essentially branched cycles that contain more than the four basic phases (isosteric and isobaric) described here.

Additional uses for the stratified storage should be explored, e.g., by integrating a domestic hot water (DHW) heat exchanger into the storage and analyzing the combined performance for space heating and DHW.

Author Contributions: Conceptualization, F.P.S. and A.S.; methodology, F.P.S. and A.S.; software, A.S.; validation, F.P.S. and A.S.; formal analysis, A.S. and F.P.S.; investigation, A.S. and F.P.S.; resources, F.P.S. and A.S.; data curation, A.S.; writing—original draft preparation, A.S.; writing—review and editing, F.P.S.; visualization, A.S.; supervision, F.P.S.; funding acquisition, F.P.S. All authors have read and agreed to the published version of the manuscript.

Funding: This research was funded by DAAD through a PhD scholarship to A.S. and by the German Federal Ministry for Economic Affairs and Climate Action (BMWK) and Projektträger Jülich (PTJ) through funding of the AdoSan-LXB project (FKZ 03ET1554).

Data Availability Statement: The detailed numerical model of the dual-adsorber cycle gas adsorption heat pump is accessible at [15]. Additionally, the numerical model for the single-adsorber cycle gas adsorption heat pump, developed within the Dymola environment as part of Alireza Sadeghlu's Ph.D. thesis, is available at the Karlsruhe Institute of Technology (KIT).

Acknowledgments: We acknowledge support by the KIT-Publication Fund of the Karlsruhe Institute of Technology.

Conflicts of Interest: The authors declare no conflict of interest.

Abbreviations

$GAHP$	Gas Adsorption Heat Pump
$SAPO-34$	Zeo-type Silico Alumino Phosphate adsorbent
$ADHX$	Adsorber/Desorber Heat Exchanger
P	Pump
V	Valve
HTS	High-Temperature Source
MTS	Medium-Temperature Sink
LTS	Low-Temperature Source
HX	Heat Exchanger
HDS	Heat Distribution System
DHW	Domestic Hot Water
HT	High Temperature
MT	Medium Temperature
LT	Low Temperature
BRN	Burner
BHX	Borehole Heat Exchanger
$\dot{m}$	Mass Flow Rate [kg/s]
T	Temperature [°C]
t	time [s]
$\frac{dS}{dt}$	Entropy Change Rate [J/K·s]
gen	generation
s	Specific Entropy [J/kg·K]
$\frac{dE}{dt}$	Energy Change Rate [W]
CV	Control Volume
$\dot{Q}$	Net Energy Transfer Rate by Heat [W]
ENV	Environment
R	Heat Transfer Resistance [K/W]
HTF	Heat Transfer Fluid
h	Specific Enthalpy [J/kg]
EC	Evaporator/Condenser
in	inlet
out	outlet
avg	average
wf	Working Fluid
h_{ads}	Specific Adsorption Enthalpy [J/kg]
RI	Relative Irreversibility [-]
tot	total

References

1. Wu, W.; Wang, B.; Shi, W.; Li, X. An overview of ammonia-based absorption chillers and heat pumps. *Renew. Sustain. Energy Rev.* **2014**, *31*, 681. [CrossRef]
2. Robur, S.p.A. Integrated Heating and Cooling Solutions with Absorption Heat Pumps Powered by Natural Gas and Renewable Energies. Available online: https://www.robur.com/products/gahp-a-heat-pump (accessed on 20 October 2024).
3. Pinheiro, J.M.; Salustio, S.; Rocha, J.; Valente, A.A.; Silva, C.M. Adsorption heat pumps for heating applications. *Renew. Sustain. Energy Rev.* **2020**, *119*, 109528. [CrossRef]
4. Demir, H.; Mobedi, M.; Ulku, S. A review on adsorption heat pump: Problems and solutions. *Renew. Sustain. Energy Rev.* **2008**, *12*, 2381–2403. [CrossRef]
5. Henninger, S.K.; Ernst, S.-J.; Gordeeva, L.; Bendix, P.; Fröhlich, D.; Grekova, A.D.; Bonaccorsi, L.; Aristov, Y.; Jaenchen, J. New materials for adsorption heat transformation and storage. *Renew. Energy* **2017**, *110*, 59–68.
6. Henninger, S.K.; Schmidt, F.P.; Henning, H.-M. Water adsorption characteristics of novel materials for heat transformation applications. *Appl. Therm. Eng.* **2010**, *30*, 1692–1702. [CrossRef]
7. Bauer, J.; Herrmann, R.; Mittelbach, W.; Schwieger, W. Zeolite/aluminum composite adsorbents for application in adsorption refrigeration. *Int. J. Energy Res.* **2009**, *33*, 1233–1249. [CrossRef]
8. Wittstadt, U.; Füldner, G.; Andersen, O.; Herrmann, R.; Schmidt, F. A new adsorbent composite material based on metal fiber technology and its application in adsorption heat exchangers. *Energies* **2015**, *8*, 8431–8446. [CrossRef]
9. Wittstadt, U.; Füldner, G.; Laurenz, E.; Warlo, A.; Große, A.; Herrmann, R.; Schnabel, L.; Mittelbach, W. A novel adsorption module with fiber heat exchangers: Performance analysis based on driving temperature differences. *Renew. Energy* **2017**, *110*, 154–161. [CrossRef]
10. Kakiuchi, H.; Shimooka, S.; Iwade, M.; Oshima, K.; Yamazaki, M.; Terada, S.; Watanabe, H.; Takewaki, T. Water vapor adsorbent FAM-Z02 and its applicability to adsorption heat pump. *Kagaku Kogaku Ronbunshu* **2005**, *31*, 273–277. [CrossRef]
11. Aristov, Y.I. Challenging offers of material science for adsorption heat transformation: A review. *Appl. Therm. Eng.* **2013**, *50*, 1610–1618.
12. Wittstadt, U.; Volmer, R.; Kleinstück, M.; Füldner, G.; Schossig, P.; Andersen, O.; Kostmann, C.; Brühling, D.; Herrmann, R.; Große, A.; et al. *Development of a Gas Adsorption Heat Pump with a Crystallized Adsorption Heat Exchanger and an Innovative Evaporator/Condenser Apparatus (ADOSO): Final Report: Project Duration: 01.05.2013-30.09.2018: 03ET1127B: Subproject B—Development of an Optimized 3D Heat Exchanger Structure for Optimized Heat and Mass Transport Processes (Fraunhofer)*; Fraunhofer-Institut für Solare Energiesysteme ISE: Freiburg, Germany, 2018. (In German) [CrossRef]
13. Laemmle, M.; Bongs, M.; Wapler, J.; Guenther, D.; Hess, S.; Kropp, M.; Herkel, S. Performance of air and ground source heat pumps retrofitted to radiator heating systems and measures to reduce space heating temperatures in existing buildings. *Energy* **2022**, *242*, 122952. [CrossRef]
14. Lämmle, M.; Metz, J.; Kropp, M.; Wapler, J.; Oltersdorf, T.; Günther, D.; Herkel, S.; Bongs, C. Heat pump systems in existing multifamily buildings: A meta-analysis of field measurement data focusing on the relationship of temperature and performance of heat pump systems. *Energy Technol.* **2023**, *11*, 2300379. [CrossRef]
15. Andersen, O.; Dörr, H.; Füldner, G.; Groddeck, P.; Herrmann, R.; Herrmann, S.; Kostmann, C.; Sadeghlu, A.; Schmalzried, H.; Schmidt, F.; et al. *AdoSan-LXB: LowEx Concepts for the Heat Supply of Multi-Family Residential Buildings; Development of a Gas Adsorption Heat Pump for Renovation of Existing Buildings: Joint Final Report: Reporting Period: 01.08.2018-28.02.2022 (FKZ 03ET1554A, B, C, E and F), 01.08.2018-30.06.2022 (FKZ 03ET1554D)*; Fraunhofer ISE: Freiburg, Germany, 2022. Available online: https://www.tib.eu/de/suchen/id/TIBKAT%3A182328843X (accessed on 24 September 2024). (In German)
16. Velte, A.; Laurenz, E.; Leisner, S.; Weber, J.; Wittstadt, U.; Füldner, G. Experimental results of a gas fired adsorption heat pump and simulative prediction of annual performance in a multi-family house. *Appl. Therm. Eng.* **2022**, *212*, 118581. [CrossRef]
17. Verein Deutscher Ingenieure (VDI). *VDI 4650 Part 2: Simplified Method for the Calculation of the Annual Heating Energy Ratio and the Annual Gas Utilisation Efficiency of Sorption Heat Pumps Gas Heat Pumps for Space Heating and Domestic Hot Water*; VDI: Düsseldorf, Germany, 2013. (In German and English)
18. Verein Deutscher Ingenieure (VDI). *VDI 4650 Part 1: Calculation of the Seasonal Coefficient of Performance of Heat Pumps Electric Heat Pumps for Space Heating and Domestic Hot Water*; VDI: Düsseldorf, Germany, 2016. (In German and English)
19. Wang, R.Z. Performance improvement of adsorption cooling by heat and mass recovery operation. *Int. J. Refrig.* **2001**, *24*, 602–611. [CrossRef]
20. Paulussen, S. Adsorption Apparatus Comprising a Heat Recovery System. U.S. Patent 20110167842A1, 14 July 2011.
21. Velte, A. Experimental Work and Development of Numerical Models for the Analysis and Optimization of Advanced Adsorption Cycles for Building Heating Supply. Ph.D. Thesis, Albert-Ludwigs-Universität, Freiburg, Germany, 2018. (In German) [CrossRef]
22. Leisner, S. Model-Based Development of a Control Algorithm for a Gas Adsorption Heat Pump with Experimental Validation. Master's Thesis, Augsburg University of Applied Sciences, Augsburg, Germany, 2021. (In German)
23. Schmidt, F.P.; Füldner, G.; Schnabel, L.; Henning, H.-M. Novel cycle concept for adsorption chiller with advanced heat recovery utilising a stratified storage. In Proceedings of the 2nd International Conference on Solar Air-Conditioning, Tarragona, Spain, 18–19 October 2007; pp. 618–623.
24. Munz, G.; Schmidt, F.; Nunez, T.; Schnabel, L. Adsorption Heat Pump with Heat Accumulator. U.S. Patent 008631667B2, 21 January 2014.

25. Schwamberger, V. Thermodynamic and Numerical Investigation of a Novel Sorption Cycle for Application in Adsorption Heat Pumps and Refrigeration Systems. Ph.D. Dissertation, Karlsruhe Institute of Technology, Karlsruhe, Germany, 2016. (In German) [CrossRef]
26. Schwamberger, V.; Desai, A.; Schmidt, F.P. Novel adsorption cycle for high-efficiency adsorption heat pumps and chillers: Modeling and simulation results. *Energies* **2020**, *13*, 19. [CrossRef]
27. Velte-Schäfer, A.; Zhang, Y.; Nonnen, T.; Wittstadt, U.; Frazzica, A.; Füldner, G.; Palomba, V. Numerical modelling and evaluation of a novel sorption module for thermally driven heat pumps and chillers using open-source simulation library. *Energy Convers. Manag.* **2023**, *291*, 117252. [CrossRef]
28. Geritzschka, M.; Lang, S.; Rieder, M.; Sirch, M.; Marx, R.; Bauer, D.; Drück, H. *Development of Large-Volume, Low-Cost Hot Water Storage Tanks with Highly Efficient Insulation for Outdoor Installation*; Universität Stuttgart–Institut für Thermodynamik und Wärmetechnik: Stuttgart, Germany, 2016. (In German)
29. van Ruth, N.J.L. New Type of Valve for Solar Thermal Storage Tank Stratification. *Energy Procedia* **2016**, *91*, 246–249. [CrossRef]
30. Wetter, M.; Zuo, W.; Nouidui, T.S.; Pang, X. Modelica Buildings library. *J. Build. Perform. Simul.* **2014**, *7*, 253–270. [CrossRef]
31. Müller, D.; Lauster, M.R.; Constantin, A.; Fuchs, M.; Remmen, P. AixLib—An Open-Source Modelica Library within the IEA-EBC Annex60 Framework. In Proceedings of the CESBP Central European Symposium on Building Physics and BauSIM 2016, Stuttgart, Germany, 14–16 September 2016; Fraunhofer IRB Verlag: Stuttgart, Germany, 2016; pp. 3–9. Available online: https://publications.rwth-aachen.de/record/681852 (accessed on 24 September 2024).
32. Wetter, M.; Blum, D.; Hu, J.; USDOE. Modelica IBPSA Library v1. May 2019. Available online: https://www.osti.gov/biblio/1529269 (accessed on 24 September 2024).
33. Bau, U.; Lanzerath, F.; Gräber, M.; Graf, S.W.; Schreiber, H.; Thielen, N.; Bardow, A. Adsorption energy systems library—Modeling adsorption based chillers, heat pumps, thermal storages and desiccant systems. In Proceedings of the 10th International Modelica Conference, Lund, Sweden, 10–12 March 2014; Modelica Association and Linkoping University Electronic Press: Lund, Sweden, 2014; Volume 96, pp. 875–883. [CrossRef]
34. Deutsches Institut für Normung (DIN). *DIN EN 12309-6: Gas-Fired Sorption Appliances for Heating and/or Cooling with a Net Heat Input Not Exceeding 70 kW—Part 6: Calculation of Seasonal Performances*; DIN: Berlin, Germany, 2015.
35. Haller, M.Y.; Cruickshank, C.A.; Streicher, W.; Harrison, S.J.; Andersen, E.; Furbo, S. Methods to determine stratification efficiency of thermal energy storage processes—Review and theoretical comparison. *Sol. Energy* **2009**, *83*, 1847–1860. [CrossRef]
36. Drück, H.; Pauschinger, T. Multiport Store–Model for TRNSYS. Type 340, Version 1.99 F. 2006. Available online: https://www.trnsys.de/static/788c19e80e1b4e690b35e44b05c8b164/ts_type_340_de.pdf (accessed on 24 September 2024).
37. Çengel, Y.A.; Boles, M.A. *Thermodynamics: An Engineering Approach*, 5th ed.; McGraw-Hill: New York, NY, USA, 2011.
38. Freni, A.; Dawoud, B.; Bonaccorsi, L.; Chmielewski, S.; Frazzica, A.; Calabrese, L.; Restuccia, G. *Characterization of Zeolite-Based Coatings for Adsorption Heat Pumps*; Springer: Berlin/Heidelberg, Germany, 2015. [CrossRef]
39. Dawoud, B. On the development of an innovative gas-fired heating appliance based on a zeolite-water adsorption heat pump; system description and seasonal gas utilization efficiency. *Appl. Therm. Eng.* **2014**, *72*, 323–330. [CrossRef]
40. Aristov, Y.I.; Sapienza, A.; Ovoshchnikov, D.S.; Freni, A.; Restuccia, G. Reallocation of adsorption and desorption times for optimisation of cooling cycles. *Int. J. Refrig.* **2012**, *35*, 525–531. [CrossRef]
41. Meunier, F.; Poyelle, F.; LeVan, M.D. Second-law analysis of adsorptive refrigeration cycles: The role of thermal coupling entropy production. *Appl. Therm. Eng.* **1997**, *17*, 43–55. [CrossRef]
42. Schmidt, F. Desai, Aditya Adsorption Heat Pump or Refrigeration Machine and Method for Its Operation. DE102018109575A1, 24 October 2019. Available online: https://register.dpma.de/DPMAregister/pat/register?AKZ=1020181095759&CURSOR=0 (accessed on 24 September 2024). (In German)